Journal of Power Sources 186 (2009) 10–21

Contents lists available at ScienceDirect

Journal of Power Sources

journal homepage: www.elsevier.com/locate/jpowsour

Geometry optimization for proton-exchange membrane fuel cells with sequential quadratic programming method

Xiu Qing Xing*, Kah Wai Lum, Hee Joo Poh, Yan Ling Wu

Institute of High Performance Computing, 1 Fusionopolis Way, #16-16 Connexis, 138632 Singapore, Singapore

ARTICLE INFO

Article history:
Received 16 May 2008
Received in revised form 5 September 2008
Accepted 9 September 2008
Available online 7 October 2008

Keywords:
Geometry optimization
Proton exchange membrane fuel cell
Sequential quadratic programming method

ABSTRACT

Integration between COMSOL Multiphysics™ and MATLAB™ offers a useful option for the self-automated geometry optimization in proton-exchange membrane fuel cells (PEMFCS). It overcomes the difficulties of automatically re-generating high-quality computational meshes and subsequently running the simulations to evaluate the objective function values using commercial software in computational fuel cell dynamics-based designs. Geometry optimization studies of an air-breathing PEMFC searching for the optimum channel ratio at the anode and the optimum open ratio at the cathode, are undertaken. A sequential quadratic programming method is selected to deal with the constrained design problems, while the objective functions are evaluated by running the three-dimensional simulation script of COMSOL™ under the MATLAB™ environment. Simulation results show that for the air-breathing PEM fuel cell operated at 353 K and one standard atmosphere pressure, when the anode channel ratio is fixed at 10%, the optimum cathode open ratios are very similar for the cell operated at voltages of 0.7 and 0.4 V, namely, 49.8% for 0.7 V and 49.5% for 0.4 V. When the cathode open ratio is set at 80% with a cell voltage of 0.7 V, the optimum anode channel ratio is found to be 34.7%.

1. Introduction

Recently, air-breathing proton-exchange membrane fuel cells (PEMFCs) have been identified as one of the most promising alternatives for traditional power sources in vehicular and portable devices. The performance of a PEMFC depends on a variety of structural and functional parameters, such as the geometry of the flow paths for the fuels, along with the operating conditions, thickness of gas distribution layers (GDL), as well as the performance of the catalyst. Studies indicate that the performance of air-breathing PEMFCs is seriously affected by oxygen mass limitation at the cathode side. To improve the performance of air-breathing PEMFCs, it is necessary to understand the relationship between the oxygen/hydrogen mass fraction distributions and the geometric designs of the cell. Numerical optimization thus becomes an important tool for understanding the physical phenomena related to various geometric configurations that affect fuel cell performance.

Unlike applications in structures and control systems, sensitivity information cannot be easily extracted from computational fluid dynamics (CFD) codes. Hence, the characteristics of the entire fuel cell, including the electrical field, the flow-field and chemical reactions, must be computed in a highly coupled manner to assess the objective function values during the fuel cell optimization design cycles. Consequently the efficiency and accuracy of the simulation are very important. CFD-based modeling of PEMFCs has been developed during the past decades [1,2]. Besides these in-house developed CFD codes, there is commercial software, such as Fluent™, Star-CD™ and COMSOL™ that can simulate fuel cell performance with reasonable accuracy.

The recent development of CFD techniques has now made it possible to carry out CFD-based optimization of the design of fuel cells. There have been several studies of the effects of functional and structural parameters on the performance of the PEM fuel cells. Wang et al. [3] investigated the influence of electrode composition on cathode performance by carrying out a series of simulations. Sinha et al. [4] found that there exists an optimum value of the diffusive length of diffusion media that provides peak performance at a given operating temperature. Hontañón et al. [5] presented a study of the performance of the flow distribution system in terms of the fuel consumption at the anode. Na and Gou [6] reported an optimization study of the efficiency and cost of a fuel cell system under various operating conditions. In addition to examinations of the effects of functional parameters, optimization of the structural parameters to maximize the performance of PEMFCs has also been performed. Sinha et al. [7] compared the performance of PEM fuel cells with parallel and serpentine flow-fields operated at elevated

* Corresponding author. Tel.: +65 64191323; fax: +65 64191580.
E-mail address: xingxq@ihpc.a-star.edu.sg (X.Q. Xing).

0378-7753/$ – see front matter © 2008 Elsevier B.V. All rights reserved.
doi:10.1016/j.jpowsour.2008.09.096

Nomenclature

c	concentration of species ($mol\,m^{-3}$)
D	diffusion coefficient ($m^2\,s^{-1}$)
E_{eq}	equilibrium voltage (V)
F	body force (N)
F	Faraday's constant (96,487 $A\,s\,mol^{-1}$)
J	transfer current density ($A\,m^{-2}$)
j_o	exchange current density ($A\,m^{-2}$)
M	molecular mass ($kg\,mol^{-1}$)
N	mass flux ($kg\,m^{-2}\,s^{-1}$)
p	pressure (Pa)
Q	source term of mass balance equations ($kg\,m^{-3}\,s^{-1}$)
R	gas constant ($J\,mol^{-1}\,K^{-1}$)
R^{agg}	agglomerate radius (m)
s	specific area (m^{-1})
S	current source term ($A\,m^{-3}$)
u	velocity vector ($m\,s^{-1}$)
x	mole fraction
x	design variable vector

Greek letters

η	dynamic viscosity ($N\,s\,m^{-2}$)
η_v	overvoltage (V)
κ	permeability (m^2)
λ	Lagrange multiplier
ρ	mixture density ($kg\,m^{-3}$)
σ	conductivity ($S\,m^{-1}$)
ϕ	potentials (V)
ω	mass fraction

Subscripts

a	anode
c	cathode
H_2	hydrogen
H_2O	water
m	membrane
O_2	oxygen
s	electrode

Superscripts

agg	agglomerate
ref	reference
T	temperature

temperature and low relative humidity. Wang et al. [8] analyzed the effect of channel configuration on air-breathing fuel cell performance by varying the widths of channels. Lin et al. [9] studied the effect of the channel-to-rib width ratio and the porosity of the GDL and the catalyst layer with a simplified conjugate-gradient method based on a two-dimensional simulation model. Hsieh and Chu [10] examined the effects of channel and rib widths on cell performance in terms of voltage–current/pressure–current curves versus flow-field pressure drop of a PEM fuel cell by experimental study. Grujicic et al. [11] combined a steady-state, single-phase electrochemical model with a non-linear constrained optimization procedure to maximize the performance of the cathode in a PEMFC. Chen et al. [12] presented a study of the internal and external structure effects on the fuel cell steady and transient operation. Cheng et al. [13] integrated a simplified conjugate-gradient method with CFD solver to determine the optimum set of geometric parameters. Mo et al. [14] reported an optimization study of PEMFCs using a hybrid genetic algorithm.

The major challenge to geometry optimization in computational fuel cell dynamics-based design lies on generating a high quality computational mesh and subsequently running the simulation to obtain the objective function through automated evaluation with commercial software. The COMSOL™ is well integrated with MATLAB™ and can be implemented in MATLAB™ as a toolbox, which offers a useful option for the self-automated geometry optimization process in PEMFCs. This study focuses on the geometry optimization, in which the effects of the anode channel ratio and the cathode open ratio on the performance of the air-breathing PEMFC are investigated in order to improve the cell performance. The sequential quadratic programming (SQP) method [15–17], being a high efficiency method, is selected to deal with the constrained design problem, while the objective function is calculated by running the 3D simulation script of COMSOL™ under the MATLAB™ environment.

2. Modeling with COMSOL™

Modeling of an air-breathing PEMFC is a challenge since the process is a multi-physics phenomenon that involves electrochemical reactions, flow dynamics in the gas channels, diffusion and convection in the GDL layer, and heat and mass transportation in porous media. In this study, a steady-state, single-phase three-dimensional model for an air-breathing PEMFC is developed using COMSOL™ to simulate the performance of the cell which is considered as the objective function value for the optimization process.

Fig. 1(a) schematically shows an air-breathing PEMFC and its various components including the membrane, the flow channels, GDLs and catalyst layers on both the anode and the cathode sides. The computational geometry is shown in Fig. 1(b). The catalyst layers at both the anode and cathode are simplified as boundaries between the GDLs and the membrane, with the thicknesses of the catalyst layers accounted in the membrane's dimension. The numerical domain computed is based on a repetitive unit of the PEMFC between the channel and the rib, and thus the external boundaries of the domain can be treated as symmetric. Air is induced into the cathode channels by virtue of natural convection, whereas hydrogen is delivered into the anode channels through forced convection. The pressures of both the air and hydrogen are set at one standard atmosphere.

Here, the applicability of the continuum theory needs to be checked since the characteristic size of the computational domain is very small. It is well known that the Knudsen number (Kn), defined as $Kn = \lambda/L$, is used to measure the ratio of the molecular mean free path length (λ) to a representative physical length scale (L). The condition $Kn \gg 1$ is called the free molecule regime, and for $Kn \ll 1$ continuum theory applies. For the particular simulation in this study, the continuum theory is valid since the Knudsen number (Kn) is at the order of 10^{-5}. Assumptions used in the model include:

(1) the Water exists in the fuel cell as vapour
(2) the electrodes and membrane are made of homogeneous materials with uniform morphological properties
(3) the cell is considered to be isothermal, i.e., the temperature distribution across the cell is uniform
(4) humid air is considered on the cathode side while only hydrogen and water vapour are considered on the anode side.

Based on the model assumptions and the scale analyses, the flow-field of reactant gases in the gas channel is governed by the continuity equation and ensures the mass conservation and the steady state incompressible Navier–Stokes equation which

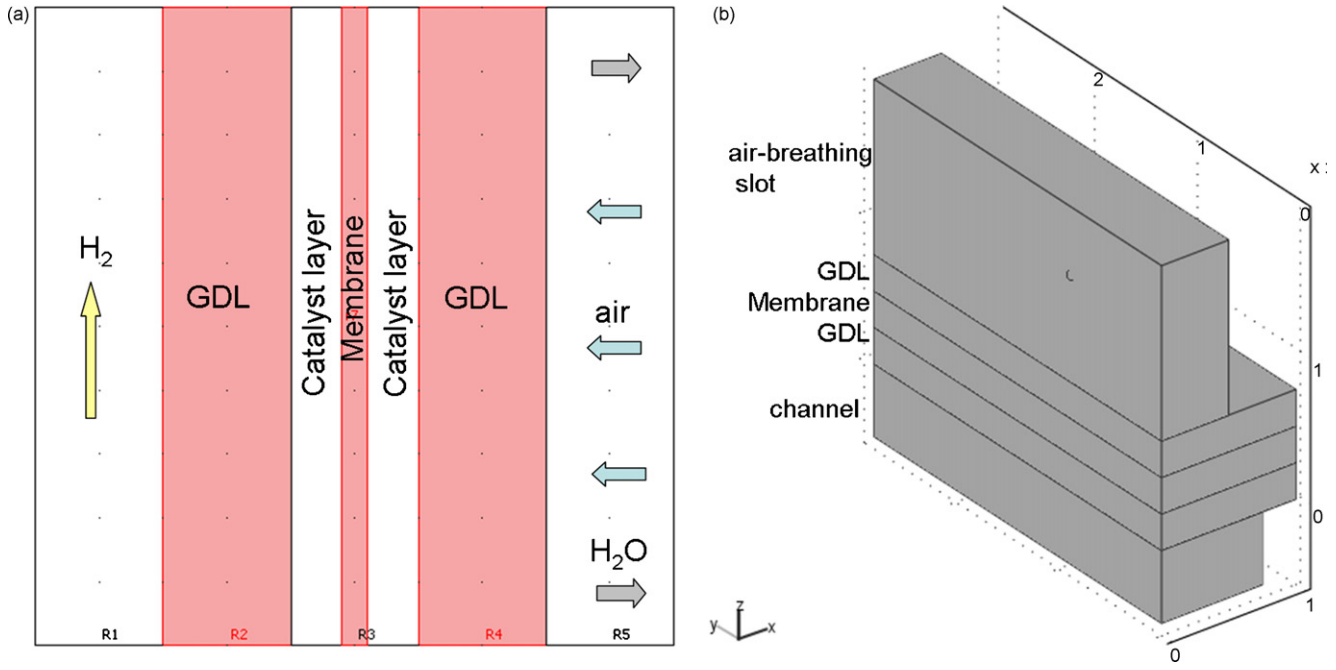

Fig. 1. Scheme of (a) air-breathing PEMFC fuel cell and (b) computational domain.

describes the momentum conservation:

$$\nabla \cdot \mathbf{u} = 0 \tag{1}$$

$$\rho \frac{D\mathbf{u}}{Dt} = -\nabla p + \mathbf{F} \tag{2}$$

where $\mathbf{u}$ is the velocity vector, p stands for pressure, $\mathbf{F}$ is the body force, and ρ is the mixture density.

The multi-component diffusion and convection phenomena are described by the Maxwell–Stafen equation, which has the general form:

$$\frac{\partial}{\partial t}\rho\omega_i + \nabla \cdot \left[-\rho\omega_i \sum_{j=1}^{N} D_{ij} \left\{ \frac{M}{M_j} \left(\nabla\omega_j + \omega_j \frac{\nabla M}{M} \right) + (x_j - \omega_j)\frac{\nabla p}{p} \right\} + \omega_i \rho \mathbf{u} + D_i^{\mathrm{T}} \frac{\nabla T}{T} \right] = Q_i \tag{3}$$

where D_{ij} is the diffusion coefficient, D^{T} is the multi-component thermal diffusion coefficient, Q_i is the source term, x is the species mole fraction, ω is the species mass fraction, T is the temperature, and M is the molecular mass. Temperature-driven diffusion is insignificant due to an assumed uniform temperature and therefore the source term Q_i is set to zero.

On the cathode side, two transport equations are solved to attain the mass fractions of oxygen and water. The mass fraction of nitrogen can be obtained from the mass balance equation:

$$\omega_{\mathrm{N_2}} = 1 - \omega_{\mathrm{O_2}} - \omega_{\mathrm{H_2O}} \tag{4}$$

Similarly, on the anode side, the transport equation of hydrogen can be solved and the mass fraction of water obtained by

$$\omega_{\mathrm{H_2O}} = 1 - \omega_{\mathrm{H_2}} \tag{5}$$

Since the GDLs are porous media, the velocity distribution is therefore formulated by Darcy's law:

$$u = -\frac{\kappa}{\eta}\nabla p \tag{6}$$

where κ is the permeability and η is the dynamic viscosity.

At the electrode-membrane boundary, the mass fluxes of hydrogen in the anode ($N_{\mathrm{H_2}}$), and of oxygen ($N_{\mathrm{O_2}}$) and water ($N_{\mathrm{H_2O}}$) in the

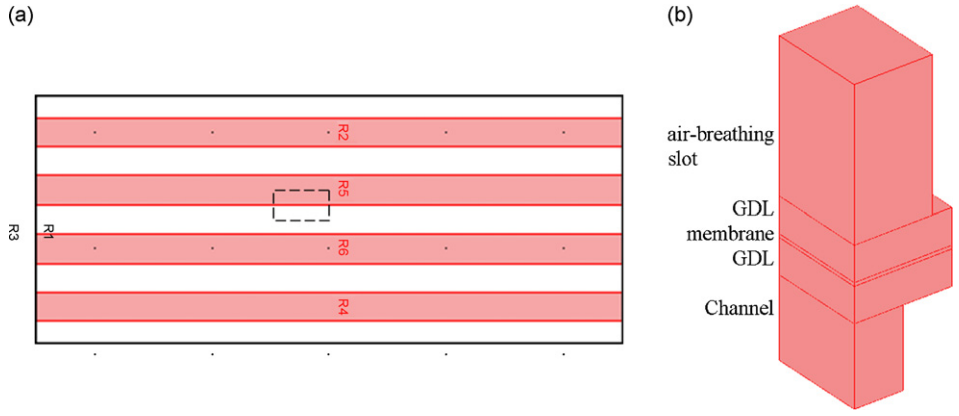

Fig. 2. Computational domain (a) top view and (b) 3D view.

Table 1
Geometry and functional parameters.

Description	Value
Anode GDL thickness	0.35 mm
Cathode GDL thickness	0.35 mm
Thickness of the membrane and catalyst layers	0.035 mm
Height of the anode channel	0.8 mm
Height of the cathode channel	1.5 mm
Anode exchange current density	1000 A m^{-2}
Cathode exchange current density	0.1 A m^{-2}
Faraday's constant	96,487 C mol^{-1}
Membrane conductivity	0.9 S cm^{-1}
Solid-phase conductivity	1250 S cm^{-1}
Porosity of GDL	0.35
Porosity of catalyst layer	0.1

cathode, are determined by the following reaction rates, respectively:

$$N_{H_2} = -\frac{j_a}{2F}M_{H_2}, \qquad N_{O_2} = -\frac{|j_c|}{4F}M_{O_2}, \qquad N_{H_2O} = \frac{|j_c|}{2F}M_{H_2O} \tag{7}$$

where j_a and j_c are the transfer current densities corresponding to the electrochemical reaction at the anode and cathode catalyst layers.

The agglomerate model describes the current density in an active layer consisting of agglomerates of ionic conductor material and electrically conducting particles covered partially with catalyst. Governing equations for the current density in the anode and cathode are

$$\begin{aligned} j_a &= -\frac{6(1-\varepsilon)FD_H^{agg}}{(R^{agg})^2}(c_H^{agg} - c_H^{ref}\exp(-\frac{2F}{RT}\eta_v)) \\ &\quad \times (1 - \sqrt{\frac{j_{o,a}s}{2Fc_H^{ref}D_H^{agg}}}R^{agg}\coth\sqrt{\frac{j_{o,a}s}{2Fc_H^{ref}D_H^{agg}}}R^{agg}) \\ j_c &= R\frac{12(1-\varepsilon)FD_O^{agg}}{(R^{agg})^2}c_O^{agg}(1 - \sqrt{\frac{j_{o,c}s(R^{agg})^2}{4Fc_O^{ref}D_O^{agg}}\exp(-\frac{0.5F}{RT}\eta_v)}) \\ &\quad \times \coth\sqrt{\frac{j_{o,c}s(R^{agg})^2}{4Fc_O^{ref}D_O^{agg}}\exp(-\frac{0.5F}{RT}\eta_v)} \end{aligned} \tag{8}$$

where D^{agg} is the agglomerate gas diffusivity, R is the gas constant, R^{agg} is the agglomerate radius, s is the specific area of the catalyst inside the agglomerate, F is the Faraday's constant, c^{ref} and c^{agg} are the reference concentrations of the species and that in the agglomerate surface, while J_o is the exchange current density, and T is the temperature. Finally, the overvoltage η_v, is defined as $\eta_v = \phi_s - \phi_m - E_{eq}$, where ϕ_s and ϕ_m are the potentials in the electrode and in the membrane, respectively. E_{eq} is the equilibrium voltage.

The conductive media direct current application mode in COMSOL™ describes the potential distributions in the solid-phase GDL and the membrane using the following equations:

$$\nabla\cdot(-\sigma_{s,eff}\nabla\phi_s) = S_s, \qquad \nabla\cdot(-\sigma_{m,eff}\nabla\phi_m) = S_m \tag{9}$$

where $\sigma_{s,eff}$ is the solid-phase effective electronic conductivity, and $\sigma_{m,eff}$ is the membrane ionic conductivity. S_s and S_m are the current source terms in the solid phase and the electrolyte phase, respectively.

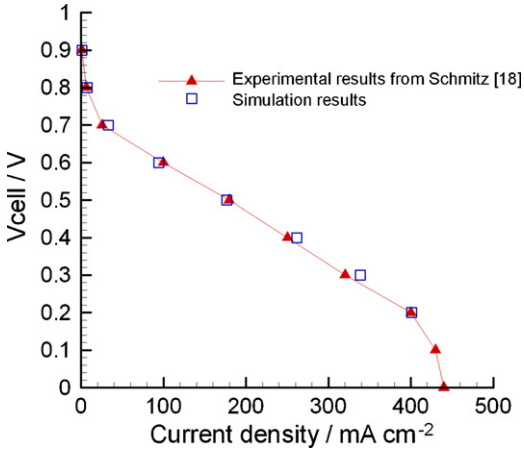

Fig. 3. Polarization curves.

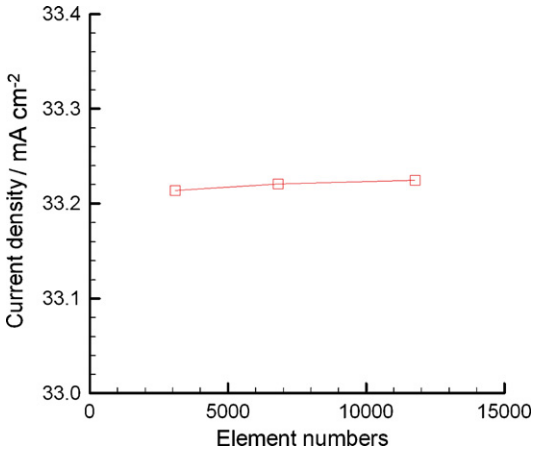

Fig. 4. Influence of grid size on cell performance.

Table 2
Geometry and functional parameters.

Description	Value
Anode GDL thickness	0.25 mm
Cathode GDL thickness	0.25 mm
Thickness of the membrane and catalyst layers	0.25 mm
Height of the anode channel	0.5 mm
Height of the cathode channel	1.2 mm
Anode exchange current density	1000 A m^{-2}
Cathode exchange current density	0.1 A m^{-2}
Faraday's constant	96,487 C mol^{-1}
Membrane conductivity	9 S cm^{-1}
Solid-phase conductivity	1000 S cm^{-1}
Permeability	10^{-13} m^2
Anode electrode potential	0 V

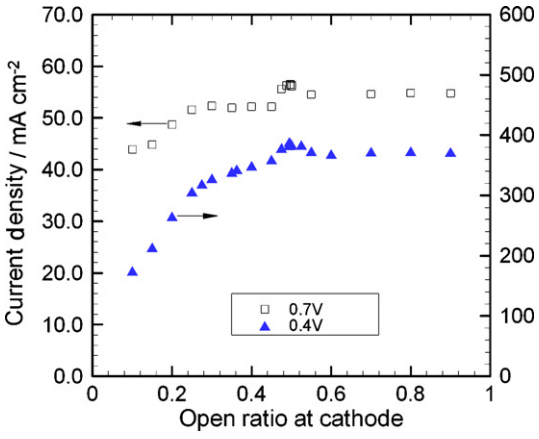

Fig. 5. Optimization convergence histories.

3. Model validation

Due to the limitation on the extensive memory requirement of COMSOL^{TM}, only a small section shown in Fig. 2(a) is selected to simulate the behaviour of the PEMFC. Thus, the computation is limited to a repetitive model between the channel and the rib. The external boundaries can be treated as symmetric. The 3D simulation domain is schematically outlined in Fig. 2(b), which consists of the cathode air-breathing slot, two GDLs, the membrane and the catalyst layers, and the anode channel for the hydrogen supply. The cathode open ratio is selected to be 80%. In order to make sure that the boundaries can be treated as symmetric, the widths of the channel and the rib are selected as 1.6 and 0.4 mm (4:1), respectively, at the cathode side, and 1 and 1 mm (1:1) for the anode side, instead of 4 and 1 mm for the cathode as designed by Schmitz et al. [18], whose experimental results are selected to validate the current model. All other geometric parameters such as the thicknesses of the GDLs and membrane, the depths of the air-breathing channel and the hydrogen anode channel, and so on, are represented by those described by Schmitz et al. [18] and are listed in Table 1. Fuel cell temperatures vary under different current conditions and Schmitz et al. [18] only reported those corresponding to two conditions, namely, 63 °C for the cell under short-circuit conditions and 43 °C at the maximum power point with the opening ratio of 80%. The temperature in this study is selected as 43 °C according to the maximum power point condition in Schmitz et al. [18]. An unstructured mesh with 3160 elements is used for this simulation. Fig. 3 shows the polarization curves obtained from the simulation and that from the experimental study by Schmitz et al. [18] at a cathode open ratio of 80%. It is found that the simulated cell performance at the maximum power point (43 °C, 0.4 V) is in reasonable agreement with the experimental results of Schmitz et al. [18],

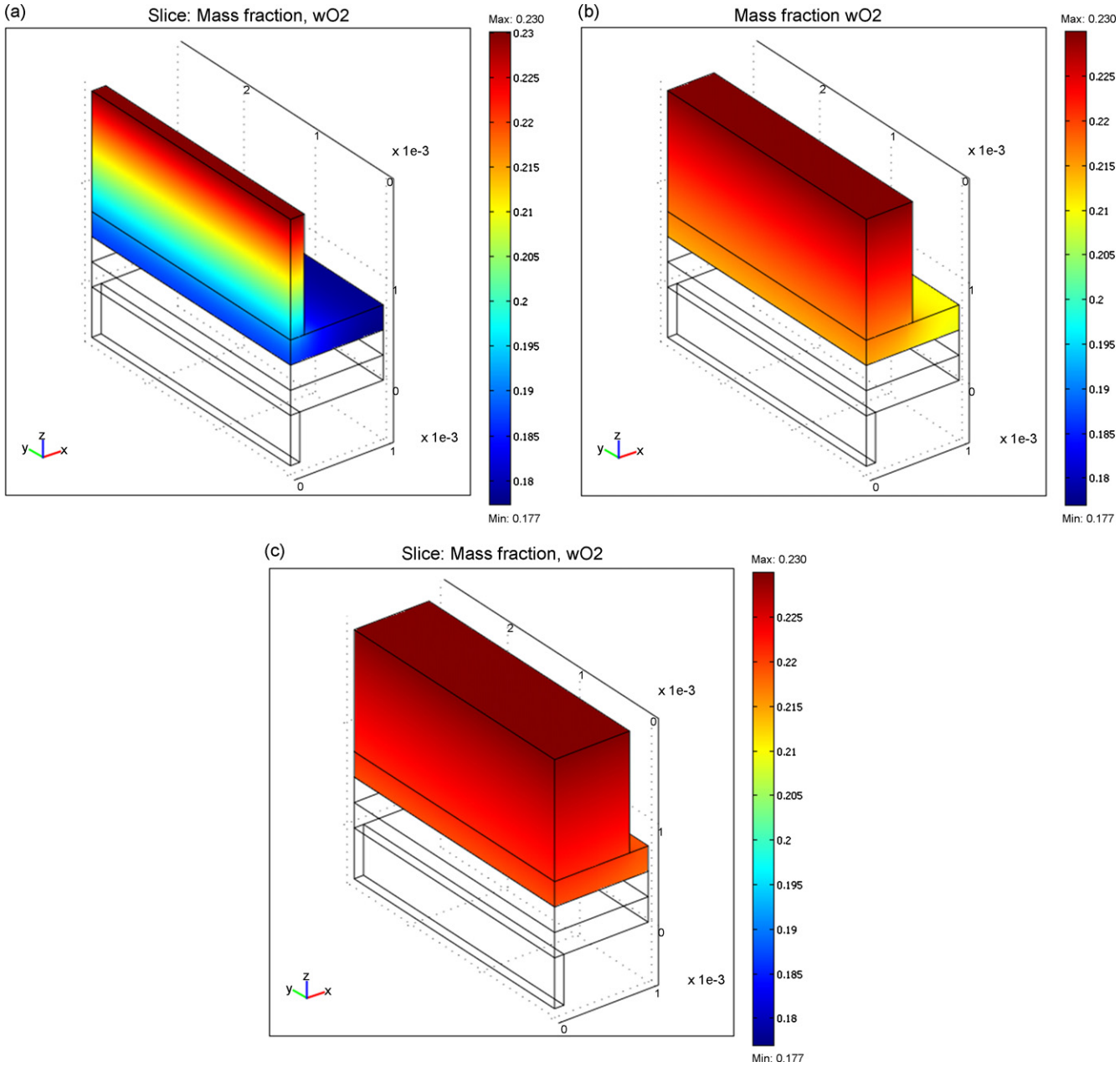

Fig. 6. Mass fraction distributions of oxygen with open ratios of (a) 15%, (b) 49.8% and (c) 80%.

indicating that the model proposed here can generate relatively accurate data.

4. Grid size independency study

The sensitivity of the converged fuel cell simulation to the size of the computational mesh is demonstrated by carrying out the simulation under the same operating conditions and consistent functional parameters for an air-breathing PEMFC, but with different mesh sizes. The grid size independence studies have been carried out with three different mesh sizes with 3085, 6811 and 11,764 elements, respectively. Fig. 4 shows the current densities obtained for the three different mesh sizes based on a cell operating at a 316 K, a cell voltage of 0.7 V, and with the cathode open ratio set at 80% (33.2136, 33.2204, and 33.2244 mA cm^{-2} corresponding to a mesh size of 3085, 6811 and 11,764, respectively). The current densities obtained with different element numbers exhibit little difference and converge to a limiting value as the number of mesh element increases. This suggests that using the coarse mesh with 3085 elements not only provides reasonably accurate results, but also saves computational costs significantly, especially when a considerable number of simulation iterations are required to evaluate the objective function values needed for the optimization processes. Therefore, the same coarse size mesh is used to evaluate the objective function values for the geometry optimization studies.

5. Optimization method

Sequential quadratic programming methods (SQP) have been developed to solve reliably constrained optimization problems with multiple variables and constraints. These methods require only a few evaluations of the objective functions and have shown

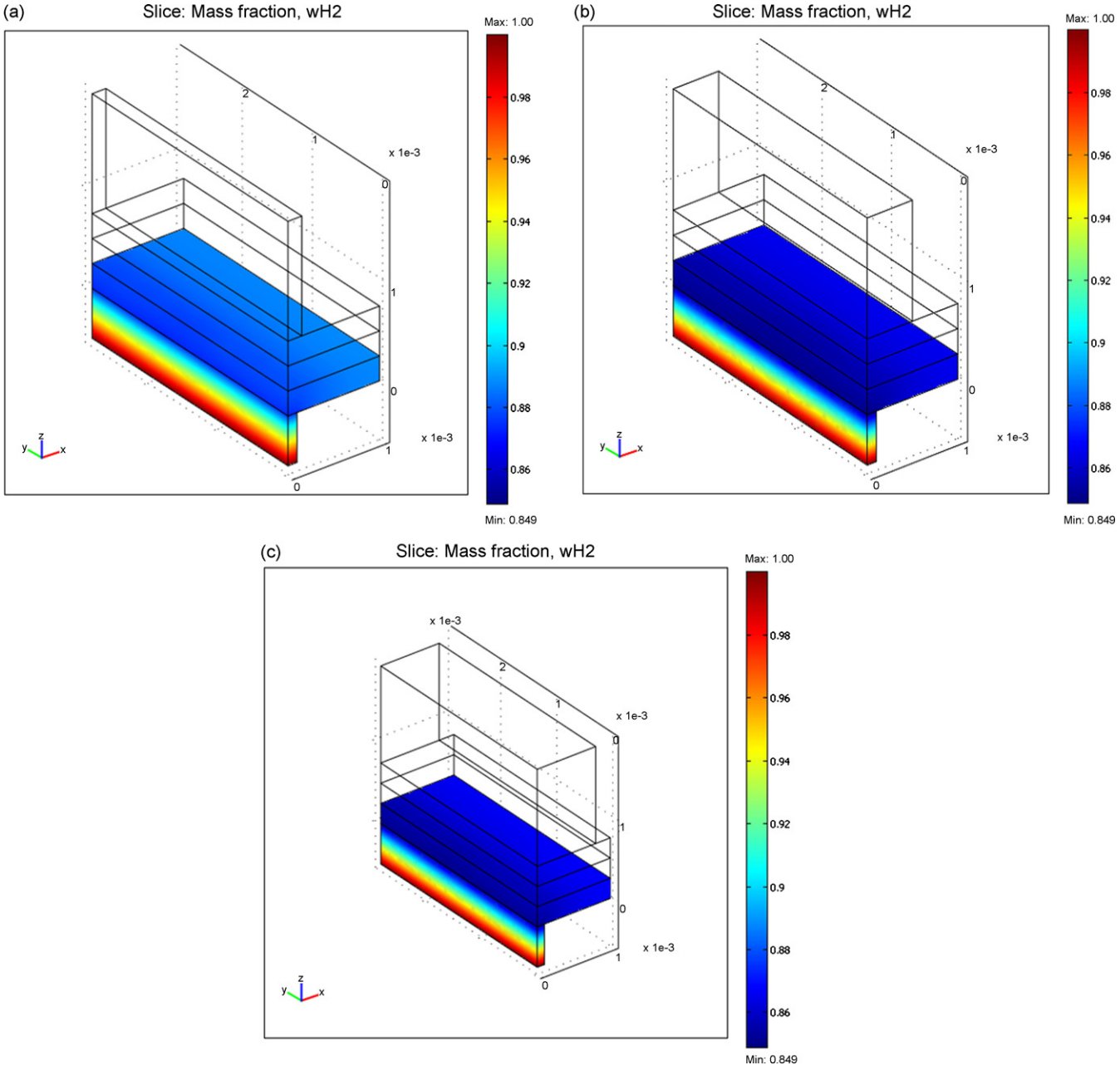

Fig. 7. Mass fraction distributions of hydrogen with open ratios of (a) 15%, (b) 49.8% and (c) 80%.

their ability in terms of accuracy and percentage of successful solutions.

The general method is stated here briefly. Given a problem described as

$$\begin{aligned} &\text{minmize} f(\mathbf{x}) \\ &\text{subject to} \\ &g_i(\mathbf{x}) = 0 \quad i = 1, \ldots, m_e \\ &g_i(\mathbf{x}) < 0 \quad i = m_e + 1, \ldots, m \end{aligned} \tag{10}$$

where, $\mathbf{x}$ is the p-dimensional vector of the design variables, $f(\mathbf{x})$ is the objective function.

The basic idea of the SQP method is to formulate a quadratic programming (QP) sub-problem based on a quadratic approximation of the Lagrangian function:

$$L(\mathbf{x}, \lambda) = f(\mathbf{x}) + \sum_{i=1}^{m} \lambda_i g_i(\mathbf{x}) \tag{11}$$

where Lagrange multipliers λ_i, $i = 1, m$ are used to balance the deviations in magnitude of the objective function and constraint gradients. Only active constraints are included in this operation, constraints that are not active excluded. Hence, Eq. (10) can be simplified by assuming that bound constraints have been expressed as inequality constraints, and the QP sub-problem is formed as

$$\begin{aligned} &\underset{d \in \Re^n}{\text{minmize}} \frac{1}{2} \boldsymbol{d}^T H_k \boldsymbol{d} + \nabla f(\mathrm{x}_k)^T \boldsymbol{d} \\ &\text{subject to} \\ &\nabla g_i(\mathbf{x}_k)^T d + g_i(\mathbf{x}_k) = 0 \quad i = 1, \ldots, m_e \\ &\nabla g_i(\mathbf{x}_k)^T d + g_i(\mathbf{x}_k) < 0 \quad i = m_e + 1, \ldots, m \end{aligned} \tag{12}$$

where H is a positive definite approximation of the Hessian matrix of the Lagrangian function (Eq. (11)), and can be updated by any of the quasi-Newton methods. $\mathbf{d}$ is the vector of the design variables of the sub-problem.

The solution of the sub-problem is used to form a new iteration:

$$\mathbf{x}_{k+1} = \mathbf{x}_k + \alpha_k \boldsymbol{d}_k \tag{13}$$

The step size parameter α_k is determined by an appropriate line search procedure so that a sufficient decrease in a merit function is obtained. $\mathbf{d}_k$ stands for the search direction.

The SQP implementation consists of three main steps namely: updating the Hessian matrix, solving the quadratic programming sub-problem, and forming the new iteration. The implementation details will not be discussed here but can be found in [15–17].

In this paper, the optimization problem is solved using the SQP algorithm in the MATLAB™ optimization toolbox to minimize the

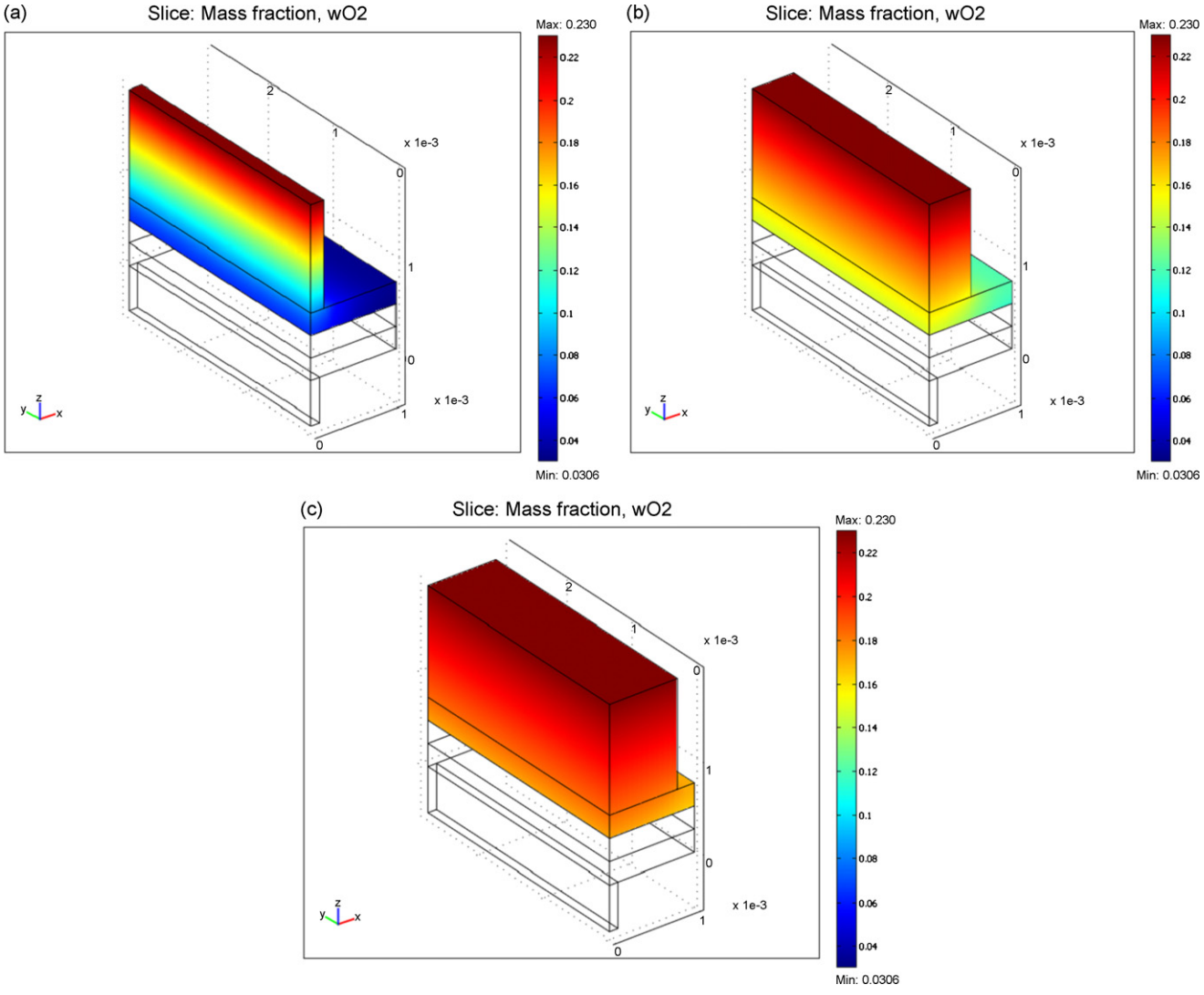

Fig. 8. Mass fraction distributions of oxygen with open ratios of (a) 15%, (b) 49.5% and (c) 80%.

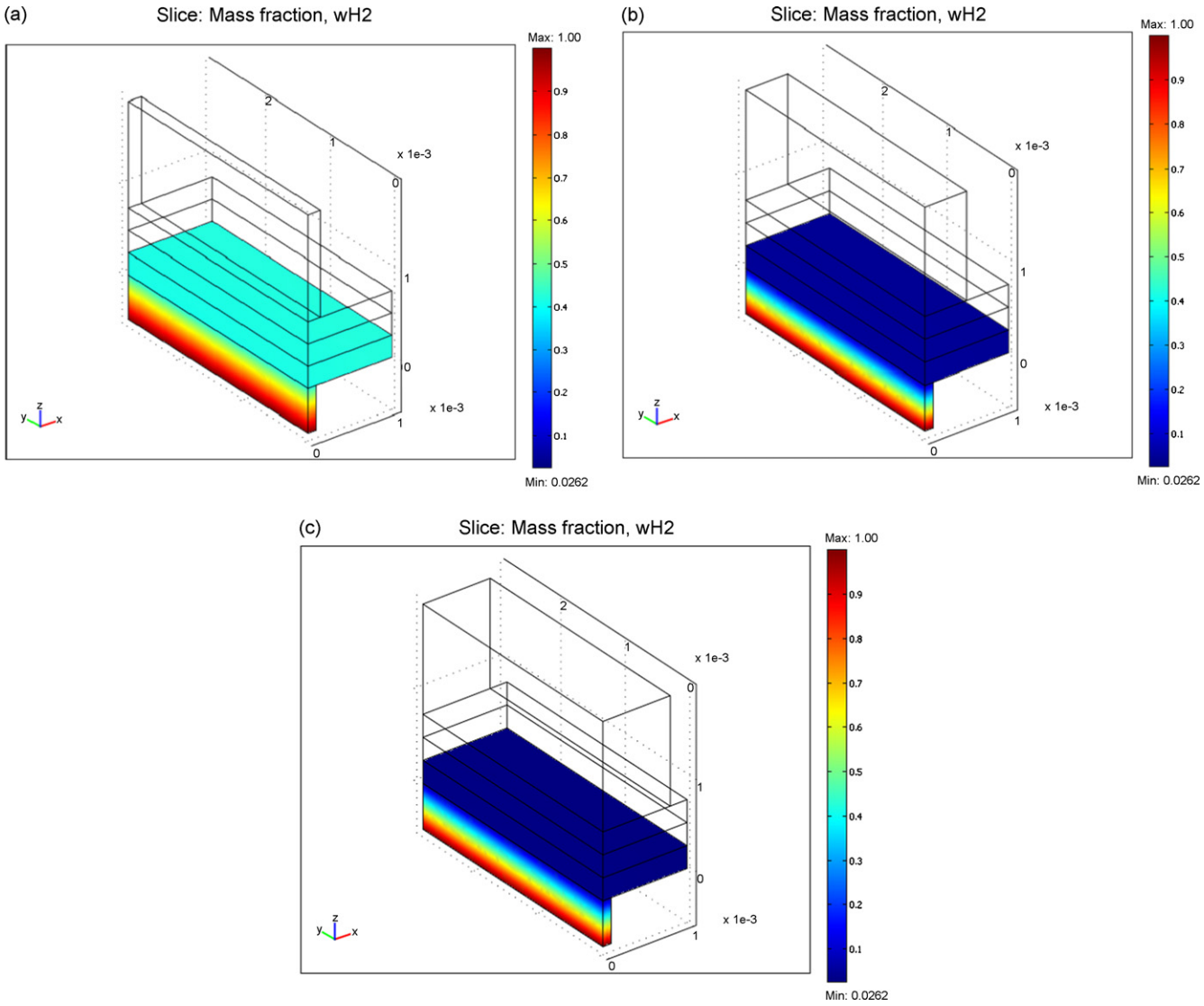

Fig. 9. Mass fraction distributions of hydrogen with open ratios of (a) 15%, (b) 49.5% and (c) 80%.

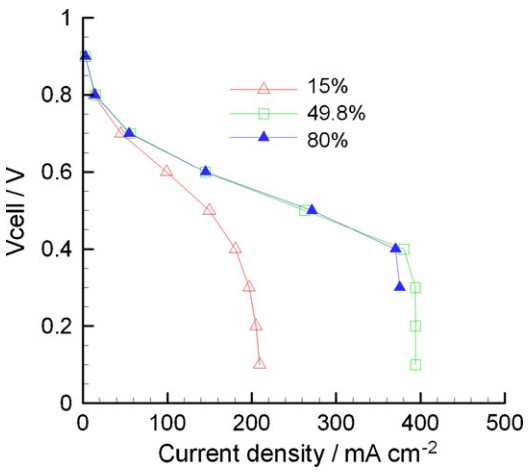

Fig. 10. Polarization curves with three different open ratios.

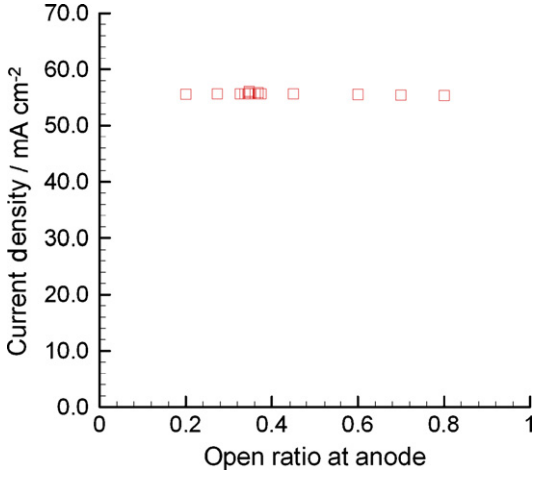

Fig. 11. Optimization convergence history.

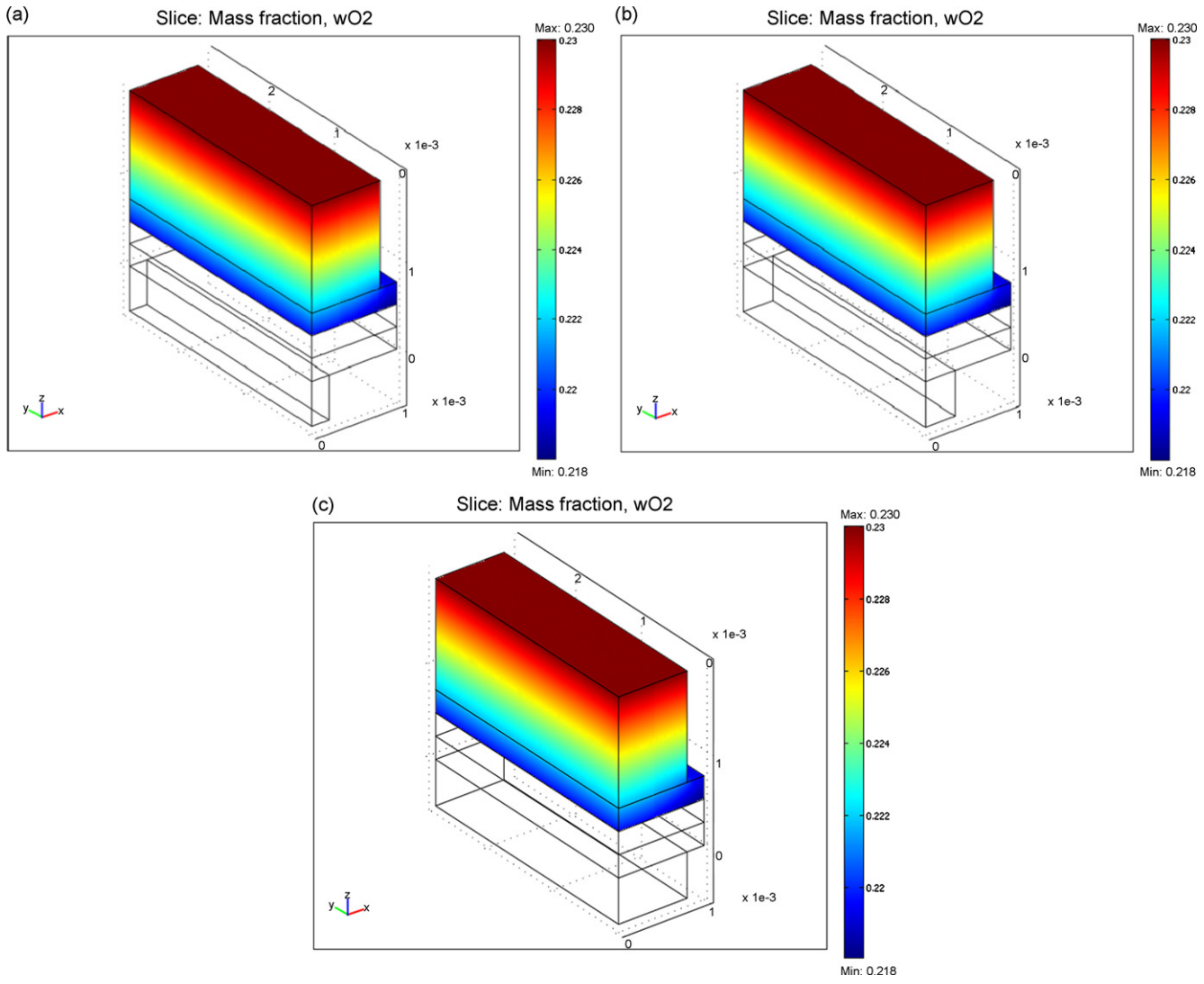

Fig. 12. Mass fraction distributions of oxygen with channel ratios of (a) 20%, (b) 34.7% and (c) 80%.

negative of the average current density at the cathode side. The objective function is evaluated by running the 3D COMSOL^{TM} simulation script under the MATLAB^{TM} environment.

6. Results and discussion

Two cases are studied to find out the optimum geometric design of the air-breathing fuel cell:

Case 1. Keeping the anode channel size constant while optimizing the cathode open ratio.
Case 2. Fixing the cathode open ratio while locating the optimum anode channel ratio.

For the above two cases, the fuel cell operating temperature is maintained at 353 K and the pressure is kept at one standard atmosphere. Cell design parameters, material properties and the functional parameters used in the simulations are listed in Table 2. The objective function is set as the current density, while the design variables are selected as the cathode open ratio for Case 1 and the anode channel ratio for Case 2, respectively. Pure hydrogen is supplied at the anode side and humidified air is supplied to the cathode side.

6.1. Case 1: optimization of cathode open ratio

Primary studies indicate that a small anode channel ratio can supply sufficient hydrogen for a cell with a relatively large cathode open ratio when the cell operates at the temperature, pressure, and the functional parameters listed in Table 2. Therefore, in Case 1, the anode channel ratio is fixed at 10%, and the cathode open ratio is set as the independent design variable. Lower and upper boundaries of the design variable are set at 10% and 90%, respectively. The current density is considered as the objective function. The values of the operating cell voltages of the fuel cell are selected as 0.7 and 0.4 V in the optimization process to determine the corresponding optimum cathode open ratios, respectively.

Since the SQP approach is a local optimization method, there are possibilities that the optimization process converges to a local optimum instead of a global result. In order to make sure that the optimization converges to a global optimal solution, the searching space is divided into a few sub-domains to guarantee that the whole spectrum of design variables (10–90%) has been searched.

Convergence histories with cell voltages at 0.7 and 0.4 V are presented in Fig. 5 with square symbols and filled delta symbols, respectively. The current density increases with enlarging the open ratio from 10% to 49.8%, and beyond 49.8% there is no significant

increment in the current density. Therefore, the optimum current density occurs at the open ratio of 49.8% at a cell voltage of 0.7 V. The optimum open ratio is found to be 49.5% when the cell voltage is fixed at 0.4 V. The convergence histories show the same trends for the two different cell voltages considered, i.e., the current density rises with the open ratio increasing from 10% to the optimum open ratio value. No obvious increment in the current density is observed with further increases in the open ratio beyond the optimum.

For a cell voltage of 0.7 V, mass fraction distributions of the oxygen at the cathode side and the hydrogen at the anode side are presented in Figs. 6 and 7 with open ratios of 15%, 49.8%, and 80%, respectively. From Fig. 6, it can be clearly seen that oxygen increases when the cathode open ratio rises from 15% to 49.8%, and further to 80% since more air is supplied to the cell. The data in Fig. 7 indicates that when the anode channel ratio is fixed at 10%, the hydrogen concentration is slightly affected by the cathode open ratio varying from 15% to 80%. This is due to the fact that as the cathode open ratio is at 15%, the oxygen supply would become the limiting factor to support the chemical reaction, leading to over-supply of hydrogen. Hence, the mass fraction of hydrogen is seen to be slightly higher than that of the other two open ratio cases while the mass fraction of the oxygen at the cathode is seen to be the lowest. As the cathode open ratio is increased, oxygen supply becomes more abundant, resulting in a higher consumption of hydrogen, and leading to a higher current density. Further increase in the open ratio beyond 49.8% results in no obvious improvement in cell performance, which suggests that when the open ratio is beyond 49.8%, hydrogen supply and oxygen supply are both sufficient, and the chemical reaction reaches a balance under the given cell volt-

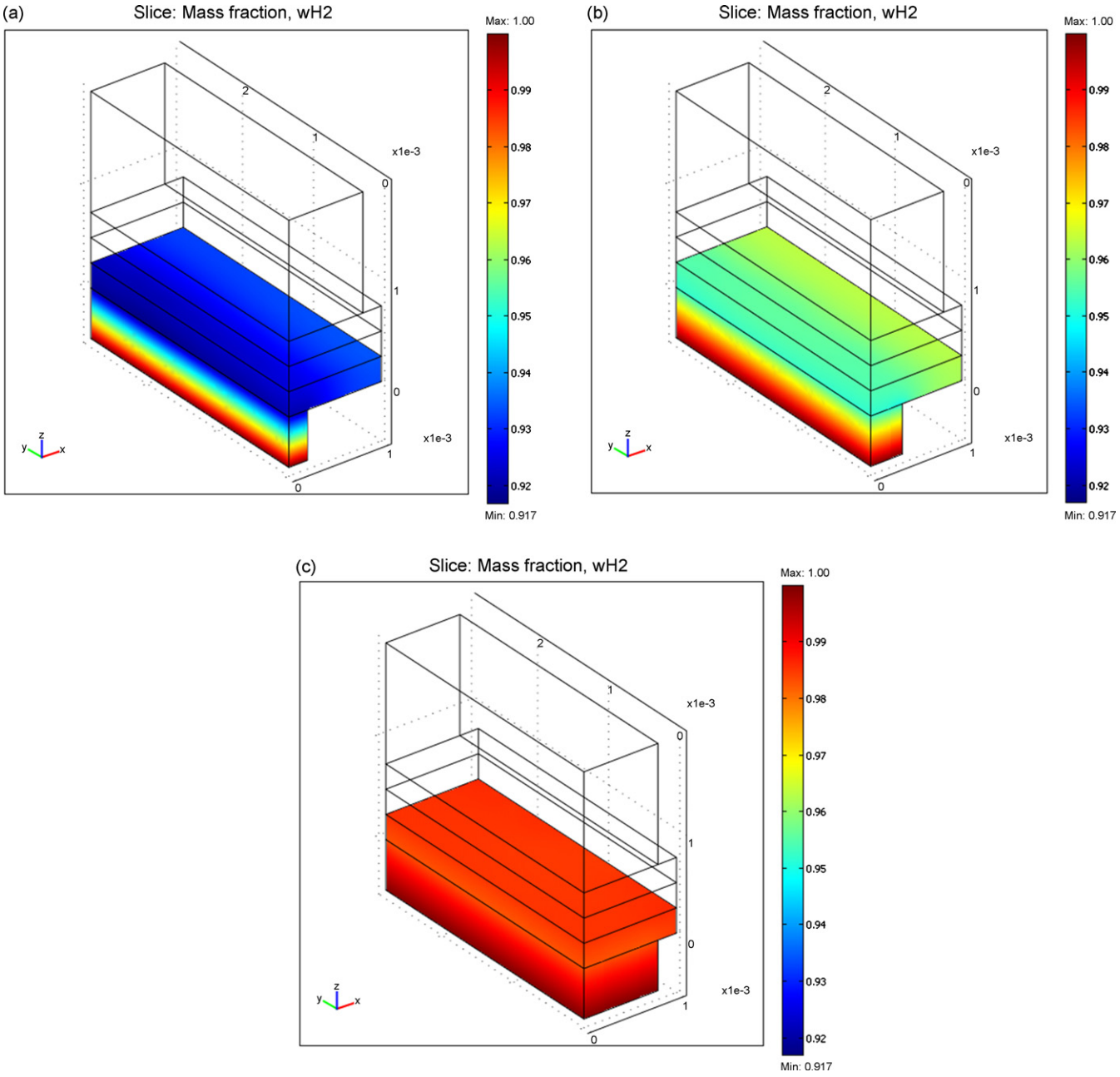

Fig. 13. Mass fraction distributions of hydrogen with channel ratios of (a) 20%, (b) 34.7% and (c) 80%.

age. Consequently, no further increment in the current density is obtained.

For a cell voltage of 0.4 V, mass fraction distributions of the oxygen at the cathode side and hydrogen at the anode side are presented in Figs. 8 and 9 with open ratios of 15%, 49.5%, and 80%, respectively. Qualitatively, a similar trend to that observed at 0.7 V is found for both oxygen and hydrogen distributions in consideration at the various cathode open ratios. However, quantitatively, the 0.4 and 0.7 V cases exhibit very different phenomena, as seen by comparing the mass fraction values of the hydrogen and the oxygen left in the GDLs and the channels or the air-breathing slots. For a cell voltage of 0.7 V, the mass fractions of the oxygen and the hydrogen left in the GDLs and the air-breathing slots or the channels are quite high when the cathode open ratio is larger or equal to 49.8%, as shown in Figs. 6 and 7. Hence for this case, cell performance is limited by the rate of the chemical reaction. For a cell voltage of 0.4 V, the data in Figs. 8 and 9 show that the mass fractions of hydrogen left in the GDL and the channel at anode are very low when the open ratio is larger or equal to 49.5%. This suggests that no further improvement in cell performance is obtained when the open ratio is beyond 49.5% since the hydrogen is depleted by the chemical reaction. Hence, for this case, the cell performance is limited by the hydrogen supply.

The polarization curves with different open ratios of 15%, 49.8% and 80% are shown in Fig. 10. It is clearly noticeable that the cell performance is very low when the open ratio is as small as 15% due to insufficient oxygen supply. The difference in cell performance between 49.8% and 80% is not significant at high operating voltages (i.e., larger or equal to 0.4 V). When the operating voltages are lower than 0.4 V, with an 80% cathode open ratio, the hydrogen supply is far from sufficient with an anode channel ratio of 10%, and consequently, maximum current occurs at 370.4 mA cm^{-2}, which is even lower than the maximum when the cathode open ratio is 49.8%.

6.2. Case 2: optimization of channel ratio at anode

In this case, the anode channel ratio is designed as the independent variable and the current density is still considered as the objective function. The operating cell voltage of the fuel cell is selected as 0.7 V in the optimization process to determine the corresponding optimum anode channel ratio.

For the same reason previously mentioned in Case 1, a relatively small anode channel ratio can supply sufficient hydrogen for a cell with a large cathode open ratio, especially when the cell voltage is as high as 0.7 V. Hence, in Case 2, the cathode open ratio is fixed at 80%. Lower and upper boundaries of the design variable (anode channel ratio) are set at 20% and 80%, respectively. The convergence history of the optimization process is presented in Fig. 11. The optimization history indicates that the optimum anode channel ratio is located at 34.7%. The variations of the current density obtained with different anode channel ratios are very small. Mass fraction distributions of the oxygen in the GDLs and the air-breathing slots are presented in Fig. 12. The mass fraction of the oxygen is seen to differ insignificantly at the different anode channel ratios of 20%, 34.7% and 80%, and the minimum mass fraction of the oxygen left in the GDLs and the slots is 0.218, which is 94.8% of the mass fraction of the oxygen in the ambient. Fig. 13 shows the mass fraction distributions of hydrogen at the anode side. It can be seen that hydrogen is present in a high amount even when the channel ratio is as low as 20%. The optimization history, together with the mass fraction distributions of the oxygen at the cathode side and the hydrogen at the anode side, indicate that the fuel supply is in abundance. The chemical reaction rate changes little with the channel ratios, and therefore results in a flat curve presented in the optimization history.

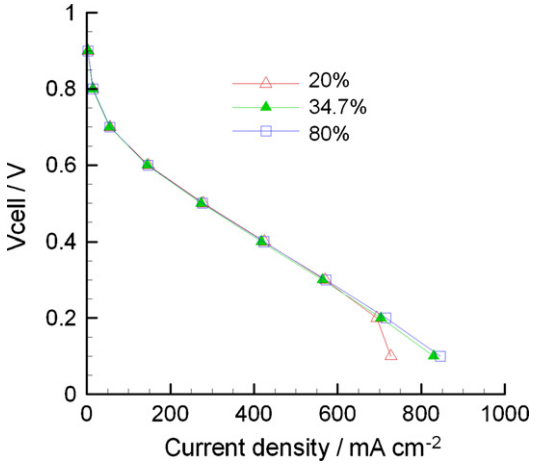

Fig. 14. Polarization curves with three different channel ratios.

Fig. 14 presents the three polarization curves, corresponding to the anode channel ratios of 20%, 34.7%, and 80%, respectively. There is insignificant difference among the three polarization curves when the cell voltage is larger than 0.2 V. Below 0.2 V, the hydrogen supply is insufficient with an anode channel ratio of 20%. The higher the anode channel ratio, the higher the current density.

Studies of the mass fraction distributions indicate that the supplies of hydrogen and oxygen are sufficient for the chemical reaction when the cathode open ratio is fixed at 80%, the anode channel ratio is greater than 20%, and the cell voltage is larger than 0.2 V. The effect of the anode channel ratios on the chemical reaction rate is negligible, leading to no significant difference among the three polarization curves.

7. Conclusion

Using the deep integration between COMSOL™ and MATLAB™, an automated geometry optimization of an air-breathing PEMFC, searching for the optimum anode channel ratio and the cathode open ratio for the enhanced fuel cell performance, is investigated. Simulation results for the air-breathing PEMFC operating at 353 K and one standard atmosphere pressure show the following:

(1) When the anode open ratio is fixed at 10%, the optimum cathode open ratios at two different operation voltages of 0.7 V and 0.4 V are rather similar, namely, 49.8% with a cell voltage of 0.7 V and 49.5% with a cell voltage of 0.4 V. Polarization curves indicate that when the cathode open ratio is less than 15%, the oxygen supply is insufficient, and results in a low cell performance. When the operating voltage is larger than or equal to 0.4 V, there is insignificant difference in the cell performance between the cathode open ratios of 49.8% and 80%. When operation voltages are lower than 0.4 V (near to the limiting current density), however, with an 80% cathode open ratio, the hydrogen supply will be depleted with a small anode channel ratio of 10%, and consequently, the cell performs worse than that with a cathode open ratio of 49.8%.

(2) When the cathode open ratio is set at 80%, the optimum anode channel ratio is found to be 34.7% at a cell voltage of 0.7 V. The optimization history, together with the mass fraction distributions of the oxygen at the cathode side and the mass fraction distributions of the hydrogen at the anode side, suggest that the fuel supply is in abundance. The rate of chemical reaction varies insignificantly with the anode channel ratio, resulting in

an asymptotic curve presented in the optimization history and little difference among the three polarization curves.

References

[1] B.R. Sivertsen, N. Djilali, J. Power Sources 141 (2005) 65–78.
[2] Y. Wang, C.Y. Wang, J. Electrochem. Soc. 152 (2005) A445–A453.
[3] G.Q. Wang, P.P. Mukherjee, C.Y. Wang, Electrochim. Acta 52 (2007) 6367–6377.
[4] P.K. Sinha, C.Y. Wang, A. Su, Int. J. Hydrogen Energy 32 (2007) 886–894.
[5] E. Hontañón, M.J. Escudero, C. Bautista, P.L. García-Ybarra, L. Dàza, J. Power Sources 86 (2000) 363–368.
[6] W. Na, B. Gou, J. Power Sources 166 (2007) 411–418.
[7] P.K. Sinha, C.Y. Wang, U. Beuscher, Int. J. Energy Res. 31 (2007) 390–411.
[8] Y. Wang, T.H. Yang, W.Y. Lee, J. Ke, C.S. Kim, J. Power Sources 145 (2005) 572–581.
[9] H.H. Lin, C.H. Cheng, C.Y. Soong, F.L. Chen, W.M. Yan, J. Power Sources 162 (2006) 246–254.
[10] S.S. Hsieh, K.M. Chu, J. Power Sources 173 (2007) 222–232.
[11] M. Grujicic, C.L. Zhao, K.M. Chittajallu, J.M. Ochterbeck, Mater. Sci. Eng. B 108 (2004) 241–252.
[12] S. Chen, J.C. Ordonez, J.V.C. Vargas, J.E.F. Gardolinski, M.A.B. Gomes, J. Power Sources 162 (2006) 356–368.
[13] C.H. Cheng, H.H. Lin, G.J. Lai, J. Power Sources 165 (2007) 803–813.
[14] Z.J. Mo, X.J. Zhu, L.Y. Wei, G.Y. Cao, Int. J. Energy Res. 30 (2006) 585–597.
[15] R. Fletcher, Practical Methods of Optimization, John Wiley and Sons, 1987, 229 pp.
[16] P.E. Gill, W. Murray, M.H. Wright, Practical Optimization, London Academic Press, 1981.
[17] W.H. Press, B.P. Flannery, S.A. Teukolsky, W.T. Vetterling, Numerical Recipes in C, The Art of Scientific Computing, Cambridge University Press, 1988, 324 pp.
[18] A. Schmitz, M. Tranitz, S. Eccarius, A. Weil, C. Hebling, J. Power Sources 154 (2006) 437–447.